Published OnlineFirst November 3, 2009; DOI: 10.1158/1535-7163.MCT-09-0255

Molecular Cancer Therapeutics

JNJ-28312141, a novel orally active colony-stimulating factor-1 receptor/FMS-related receptor tyrosine kinase-3 receptor tyrosine kinase inhibitor with potential utility in solid tumors, bone metastases, and acute myeloid leukemia

Carl L. Manthey, Dana L. Johnson, Carl R. Illig, et al.

Mol Cancer Ther 2009;8:3151-3161. Published OnlineFirst November 3, 2009.

Published OnlineFirst November 3, 2009; DOI: 10.1158/1535-7163.MCT-09-0255

JNJ-28312141, a novel orally active colony-stimulating factor-1 receptor/FMS-related receptor tyrosine kinase-3 receptor tyrosine kinase inhibitor with potential utility in solid tumors, bone metastases, and acute myeloid leukemia

Carl L. Manthey, Dana L. Johnson, Carl R. Illig, Robert W. Tuman, Zhao Zhou, Judith F. Baker, Margery A. Chaikin, Robert R. Donatelli, Carol F. Franks, Lee Zeng, Carl Crysler, Yanmin Chen, Edward J. Yurkow, Lisa Boczon, Sanath K. Meegalla, Kenneth J. Wilson, Mark J. Wall, Jinsheng Chen, Shelley K. Ballentine, Heidi Ott, Christian Baumann, Danielle Lawrence, Bruce E. Tomczuk, and Christopher J. Molloy

Johnson & Johnson Pharmaceutical Research & Development, L.L.C., Spring House, Pennsylvania

Abstract

There is increasing evidence that tumor-associated macrophages promote the malignancy of some cancers. Colony-stimulating factor-1 (CSF-1) is expressed by many tumors and is a growth factor for macrophages and mediates osteoclast differentiation. Herein, we report the efficacy of a novel orally active CSF-1 receptor (CSF-1R) kinase inhibitor, JNJ-28312141, in proof of concept studies of solid tumor growth and tumor-induced bone erosion. H460 lung adenocarcinoma cells did not express CSF-1R and were not growth inhibited by JNJ-28312141 *in vitro*. Nevertheless, daily p.o. administration of JNJ-28312141 caused dose-dependent suppression of H460 tumor growth in nude mice that correlated with marked reductions in F4/80$^+$ tumor-associated macrophages and with increased plasma CSF-1, a possible biomarker of CSF-1R inhibition. Furthermore, the tumor microvasculature was reduced in JNJ-28312141–treated mice, consistent with a role for macrophages in tumor angiogenesis. In separate studies, JNJ-28312141 was compared with zoledronate in a model in which MRMT-1 mammary carcinoma cells inoculated into the tibias of rats led to severe cortical and trabecular bone lesions. Both agents reduced tumor growth and preserved bone. However, JNJ-28312141 reduced the number of tumor-associated osteoclasts superior to zoledronate. JNJ-28312141 exhibited additional activity against FMS-related receptor tyrosine kinase-3 (FLT3). To more fully define the therapeutic potential of this new agent, JNJ-28312141 was evaluated in a FLT3-dependent acute myeloid leukemia tumor xenograft model and caused tumor regression. In summary, this novel CSF-1R/FLT3 inhibitor represents a new agent with potential therapeutic activity in acute myeloid leukemia and in settings where CSF-1–dependent macrophages and osteoclasts contribute to tumor growth and skeletal events. [Mol Cancer Ther 2009;8(11):3151–61]

Introduction

Tumor-associated macrophages (TAM) comprise 5% to 50% of cells in many tumors (1). Numerous studies report positive correlations between numbers of TAMs, angiogenesis, and tumor progression (reviewed in ref. 2). In response to tumor microenvironments, macrophages elaborate growth factors, and immune suppressive cytokines (3, 4), and a growing body of evidence suggests macrophages promote tumor angiogenesis and progression (5–12). Several preclinical studies have shown tumor growth suppression by chemical or genetic depletion of TAMs (8–12).

The macrophage lineage is dependent, in large part, on colony-stimulating factor-1 (CSF-1). CSF-1 mediates tissue macrophage recruitment and survival and the proliferation and differentiation of macrophage precursors both locally and in bone marrow (13). Mice lacking a functional CSF-1 gene or a functional CSF-1 receptor (CSF-1R) gene have marked deficits in macrophage numbers in several tissues (14, 15). Of particular relevance, TAM numbers were greatly reduced in developing mammary carcinomas in CSF-1–deficient mice compared with carcinomas in mice with normal CSF-1 expression (6). A role for CSF-1–dependent TAMs in tumor growth was first inferred by the poor growth of Lewis lung carcinomas in CSF-1–deficient mice (7), whereas parenteral administration of recombinant CSF-1 accelerated tumor growth in wild-type mice (16). CSF-1 antisense oligonucleotides or neutralizing antibody have reduced the growth rates of colon, germline, and mammary carcinoma xenografts (10–12). Tumor growth suppression was associated with reduce TAMs together with diminished expression of vascular endothelial

Received 3/18/09; revised 8/21/09; accepted 9/27/09; published OnlineFirst 11/3/09.

The costs of publication of this article were defrayed in part by the payment of page charges. This article must therefore be hereby marked *advertisement* in accordance with 18 U.S.C. Section 1734 solely to indicate this fact.

Note: Supplementary material for this article is available at Molecular Cancer Therapeutics Online (http://mct.aacrjournals.org/).

Requests for reprints: Carl L. Manthey, Johnson & Johnson Pharmaceutical Research & Development, Welsh and McKean Roads, Spring House, PA 19477. Phone: 215-628-8134; Fax: 215-540-4627.
E-mail: cmanthey@its.jnj.com

doi:10.1158/1535-7163.MCT-09-0255

Published OnlineFirst November 3, 2009; DOI: 10.1158/1535-7163.MCT-09-0255

growth factor, matrix metalloproteases, and reduced tumor vasculature.

The majority of patients suffering late-stage breast and prostate cancer will progress to metastatic bone disease. Many will experience tumor-induced bone erosions sufficient to cause pain, fracture, or hypercalcemia despite bisphosphonate therapy (17). CSF-1, together with RANK ligand, is required for osteoclastogenesis, as illustrated by the near absence of osteoclasts in CSF-1–deficient or CSF-1R–deficient mice (14, 15). CSF-1 is expressed by tumors, and metastatic bone disease has been linked to elevated plasma CSF-1 (18–21).

Taken together, inhibition of CSF-1 seems a promising experimental approach to treat patients with solid tumors and metastatic bone disease. The CSF-1R (also known as FMS) is a member of the type III family of receptor tyrosine kinases, and the kinase domain of CSF-1R offers a tractable drug site. Toward this end, we optimized small molecule inhibitors of CSF-1R kinase (22–24). Among these, JNJ-28312141 was selected for preclinical proof-of-concept studies. We investigated the ability of JNJ-28312141 to suppress the *in vivo* growth of H460 non–small cell lung adenocarcinoma xenografts and to prevent bone erosions by syngeneic MRMT-1 mammary carcinoma. JNJ-28312141 also inhibited the closely related FMS-like receptor tyrosine kinase-3 (FLT3). Because a subset of acute myeloid leukemia (AML) is FLT3 dependent (25–27), the ability of JNJ-28312141 to regress MV-4-11 AML xenografts was assessed to more fully define the therapeutic potential of this new agent.

Materials and Methods

JNJ-28312141, 4-cyano-*N*-[2-(1-cyclohexen-1-yl)-4-[1-[(dimethylamino)acetyl]-4-piperidinyl]phenyl]-1*H*-imidazole-2-carboxamide monohydrochloride, was prepared as described (22).

Kinase Assays

Assays used to determine the IC_{50} values for CSF-1R, FLT3, KIT, AXL, and TRKA were carried out using a fluorescence polarization competition immunoassay format and have been described previously (23). Briefly, for CSF-1R, CSF-1R(538–972) encompassing the tyrosine kinase domain was expressed and purified from a baculovirus system (28). The CSF-1R kinase assay measured phosphorylation of tyrosine residues present on a synthetic peptide (SYEGNSYTFIDPTQ) equivalent to CSF-1R(555–568). Final concentrations in the 10-μL reaction mixture were 100 mmol/L HEPES (pH 7.5), 1 mmol/L DTT, 0.01% Tween 20, 2% DMSO, 308 μmol/L SYEGNSYTFIDPTQ, 1 mmol/L ATP, 5 mmol/L $MgCl_2$, and 0.7 nmol/L CSF-1R(538–972). The reaction was initiated by adding ATP. The plates were incubated at room temperature for 80 min. Reactions were stopped by addition of 1.2 μL of 50 mmol/L EDTA. Each well received 10 μL of a 1:1:3 mixture of 10× anti-phosphotyrosine antibody, 10× PTK green tracer, and fluorescence polarization dilution buffer (Invitrogen). After 30 min at room temperature, fluorescence polarization was read (485 nm excitation, 530 nm emission) on an Analyst plate reader (Molecular Devices). Fluorescence polarization values for maximum (5 mmol/L EDTA) and minimum (DMSO) inhibition were used to define 100% and 0% inhibition.

The IC_{50} for LCK and the inhibition of 59 kinases at 1 and 0.1 μmol/L were determined using the Invitrogen SelectScreen Kinase Profiling Service. Fifty-seven additional kinases were assayed using the Millipore KinaseProfiler Assay Service.

Cell Assays

Inhibition of CSF-1–induced CSF-1R phosphorylation was measured using HEK293 cells transfected to express wild-type CSF-1R and an immunoblot assay described previously (29). A similar approach was used to measure inhibition of FLT3 ligand–induced FLT3 phosphorylation in Baf3 cells transfected to express FLT3 and GAS6-induced AXL phosphorylation in HEK293 cells transfected to express AXL.

Functional inhibition of CSF-1R was determined by assaying CSF-1–driven mouse macrophage proliferation and MCP-1 production by human monocytes. Monocytes were isolated from human blood using RosetteSep human monocyte enrichment cocktail (StemCell Technologies) and were plated (2×10^5 per well) into round-bottomed 96-well polypropylene plates with RPMI 1640 containing 10% heat-inactivated fetal bovine serum (FBS) and graded concentrations of JNJ-28312141. Cells were stimulated 16 h with 100 ng/mL recombinant human CSF-1 (R&D Systems), and secreted MCP-1 was measured by ELISA (R&D Systems). Mouse macrophages were derived from bone marrow as described (23). Macrophages suspended in EMEM containing 10% FBS were plated at a density of 5,000 cells per well into Costar 96-well tissue culture plates. After overnight culture, wells were adjusted to contain 5 ng/mL CSF-1, 1 μmol/L indomethacin, and graded concentrations of JNJ-28312141. Twenty-four hours later, wells were adjusted to contain bromodeoxyuridine for an additional 6 h. Incorporation of bromodeoxyuridine into the DNA of proliferating macrophages was quantified by ELISA (Exalpha Corp.).

Cell proliferation dependent on FLT3, KIT, and TRKA was assessed using MV-4-11 AML cells (ATCC CRL-9591), Mo7e erythroleukemia cells (DSMZ ACC-104), and TF-1 myeloid leukemia cells (ATCC CRL-2003), respectively. Cells were dispensed into microtiter plates (10,000 per well) together with graded concentrations of JNJ-28312141. Mo7e and TF-1 cultures were adjusted to contain 25 ng/mL stem cell factor or 1.4 ng/mL nerve growth factor, respectively. MV-4-11 cells were growth factor independent, due to an internal tandem duplication (ITD) of the FLT3 juxtamembrane domain, rendering FLT3 constitutively active (21). After a 72-h culture period, relative cell numbers were determined using CellTiterGlo reagent (Promega). MV-4-11 growth was calculated based on the difference between luminescence on day 3 versus day 0. M-07e and TF-1 growth was calculated based on the difference in luminescence of cells cultured in the presence versus the absence of growth factor.

Published OnlineFirst November 3, 2009; DOI: 10.1158/1535-7163.MCT-09-0255

Animal Studies

Animals were housed in facilities fully accredited by the American Association for Assessment and Accreditation of Laboratory Animal Care, and procedures were conducted in compliance with the NIH Guide for the Care and Use of Laboratory Animals.

CSF-1–Induced c-fos Pharmacodynamic Model

Groups of six B6C3F1 mice (Taconic Farms), 8 wk of age, were dosed (p.o.) with vehicle [aqueous 20% hydroxypropyl-β-cyclodextrin (HPβCD)] or JNJ-28312141 or dosed i.p. with 0.2 μg of rat monoclonal anti-mouse CSF-1 antibody (clone 5A1, BD Bioscience) or 0.2 μg of isotype (IgG1κ) control antibody. Eight hours later, mice were given saline or 0.8 μg recombinant mouse CSF-1 (Cell Biosciences, Inc.) via the tail vein. Fifteen minutes after the tail vein injection, mice were euthanized. RNA was extracted from spleens using Trizol reagent (Invitrogen) and purified further using RNeasy columns (Qiagen). Relative expression of c-fos mRNA in spleens of mice dosed with vehicle or JNJ-28312141 was determined by reverse transcription–PCR as described (24).

NCI-H460 Human Lung Tumor Xenograft Model

NCI-H460 human non–small cell lung adenocarcinoma cells (American Type Culture Collection) were suspended at 1×10^7 cells/mL in sterile PBS, and 100 μL were injected s.c. into the left inguinal region of female (9–10 wk old) CD-1 *nu/nu* mice (Charles River). Three days later, mice were randomized into four groups (15 per group) and p.o. gavage dosing was initiated with vehicle (HPβCD) or with JNJ-28312141 at doses of 25, 50, and 100 mg/kg. Dosing was twice daily during the week and once daily on weekends for 25 consecutive days. Tumor volumes were determined using Vernier calipers and the formula $(L \times W)^2/2$, where L is length (mm) and W is width (shortest distance in mm) of the tumor. At study termination, blood samples were collected into heparin-coated tubes by cardiac puncture under CO_2 anesthesia. Plasma was analyzed for human and mouse CSF-1 using specific ELISAs (R&D Systems). Half of each tumor was snap frozen in Tissue-Tek optimal cutting temperature media (VWR). To assess vessel density, 8-μm cryostat sections were fixed 5 min in cold acetone, air-dried, blocked with 5% goat serum in PBS, and blocked further with avidin-biotin solution (Vector Corporation). After washing, the sections were covered with PBS containing 10 μg/mL rat anti-mouse CD31 (Caltag Laboratories) for 60 min, washed, and stained using the ABC-AP Rat kit (Vector Corporation). Rat IgG (Caltag Laboratories) was used as a negative control and was negative in all cases. The sections were lightly counterstained (H&E), and the percentage of tumor area occupied by vessels was calculated at 40× magnification using Image Pro Plus (Phase 3 Image) image analysis software. The other half of each tumor was fixed in 10% formalin and paraffin embedded. Five-micrometer sections were stained using rat anti-mouse F4/80 (Clone C1:A3-1, Serotec) and a horseradish peroxidase detection system (Dako Cytomation) composed of biotinylated rabbit anti-rat immunoglobulin, anti-rabbit Envision with labeled polymer–horseradish peroxidase, and 3,3′-diaminobenzidine. For each tumor, the three areas of highest macrophage density were assessed at 100× magnification. The percentage of each field positive for F4/80-stained cells was determined with the aid of Image Pro Plus software, and the three fields were averaged for each tumor.

Rat MRMT-1 Bone Metastasis Model

A rat mammary MRMT-1 adenocarcinoma bone metastasis model (30, 31) was done by MDS Pharma Services. Female Sprague-Dawley rats (Harlan Sprague-Dawley; ~125–150 g) were acclimated for 1 wk. As described (31), MRMT-1 cells (3×10^4) were inoculated into the medullary cavity of the right proximal tibia. Groups of inoculated rats ($n = 8$) were dosed on days 3–16, twice daily by p.o. gavage with vehicle (0.5% hydroxypropyl-methylcellulose) or JNJ-28312141 at 20 or 60 mg/kg. For comparison, a fourth group was given 0.03 mg/kg zoledronate in saline by s.c. injection every other day beginning on day 3. Rats were sacrificed on day 17. Right hind limbs were excised with surrounding tumor tissue, and microradiographs were prepared using an MX-20 X-ray system (Faxitron X-ray Corporation). Microradiographs were scored for tumor-induced osteolysis as follows: 0, no signs of destruction; 1, one to three small radiolucent lesions; 2, three to six lesions and loss of medullary bone; 3, loss of medullary bone and erosion of cortical bone; 4, full thickness unicortical bone loss; 5, full thickness bicortical bone loss and/or displaced skeletal fracture. The radiographs were used to select representative hind limbs from each group for microcomputed tomography imaging. All hind limbs were fixed in 10% neutral buffered formalin, decalcified, and paraffin-embedded. Sections (8 μm) were stained for tartrate-resistant alkaline phosphate–positive ($TRAP^+$) osteoclasts as described (32). For each tibia, tumor-associated $TRAP^+$ osteoclasts were counted in three fields (200×) with highest osteoclast frequency and averaged. A three-point method was used to score tibia sections for trabecular bone volume (3, >40% marrow area; 2, >10% and <40% marrow area; 1, 1–10% marrow area; 0, none) and tumor volume (3, large; 2, moderate; 1, small; 0, none).

MV-4-11 AML Human Xenograft Model

MV-4-11 cells were suspended at 2.5×10^7/mL in a 1:1 mixture of PBS/Matrigel, and 0.2 mL was injected s.c. into the left inguinal region of female (9–10 wk old) CD-1, *nu/nu,* mice (Charles River). Three weeks later, mice bearing tumors ranging in size from 100 to 586 mm^3 (mean tumor volume, 288 mm^3) were randomized (15 per group) and dosed with vehicle (HPβCD) or JNJ-28312141 at 10, 50, or 100 mg/kg for 11 d. Dosing was p.o. twice daily except once daily on weekends. Tumor volumes were measured as described for H460 xenografts. Phosphorylated FLT3 was assessed as described (26). Briefly, FLT3 was immunoprecipitated overnight from tumor lysates using agarose-conjugated anti-FLT3 antibody (Santa Cruz Biotechnology Corp.). Immunoprecipitates were resolved by SDS-PAGE and blotted onto nitrocellulose membranes. pFLT3 was detected with a horseradish peroxidase–conjugated phosphotyrosine antibody (Clone 4G10, Upstate Biotechnology). Total FLT3

Published OnlineFirst November 3, 2009; DOI: 10.1158/1535-7163.MCT-09-0255

was detected on a replicate membrane using anti-FLT3 antibody (Santa Cruz Biotechnology Corp.).

Statistical Analysis

Differences between treated and vehicle control animals were analyzed statistically by ANOVA and Dunnett's *t* test, with a *P* value of ≤0.05 (two-tailed) considered statistically significant.

Results

JNJ-28312141 Is a Potent Inhibitor of CSF-1R with a Narrow Kinase Selectivity Profile

JNJ-28312141 (Fig. 1A) was a product of a medicinal chemistry campaign to optimize inhibitors of CSF-1R kinase (22–24). JNJ-28312141 had an IC_{50} value of 0.00069 μmol/L in an assay of CSF-1R kinase activity. Specificity for CSF-1R

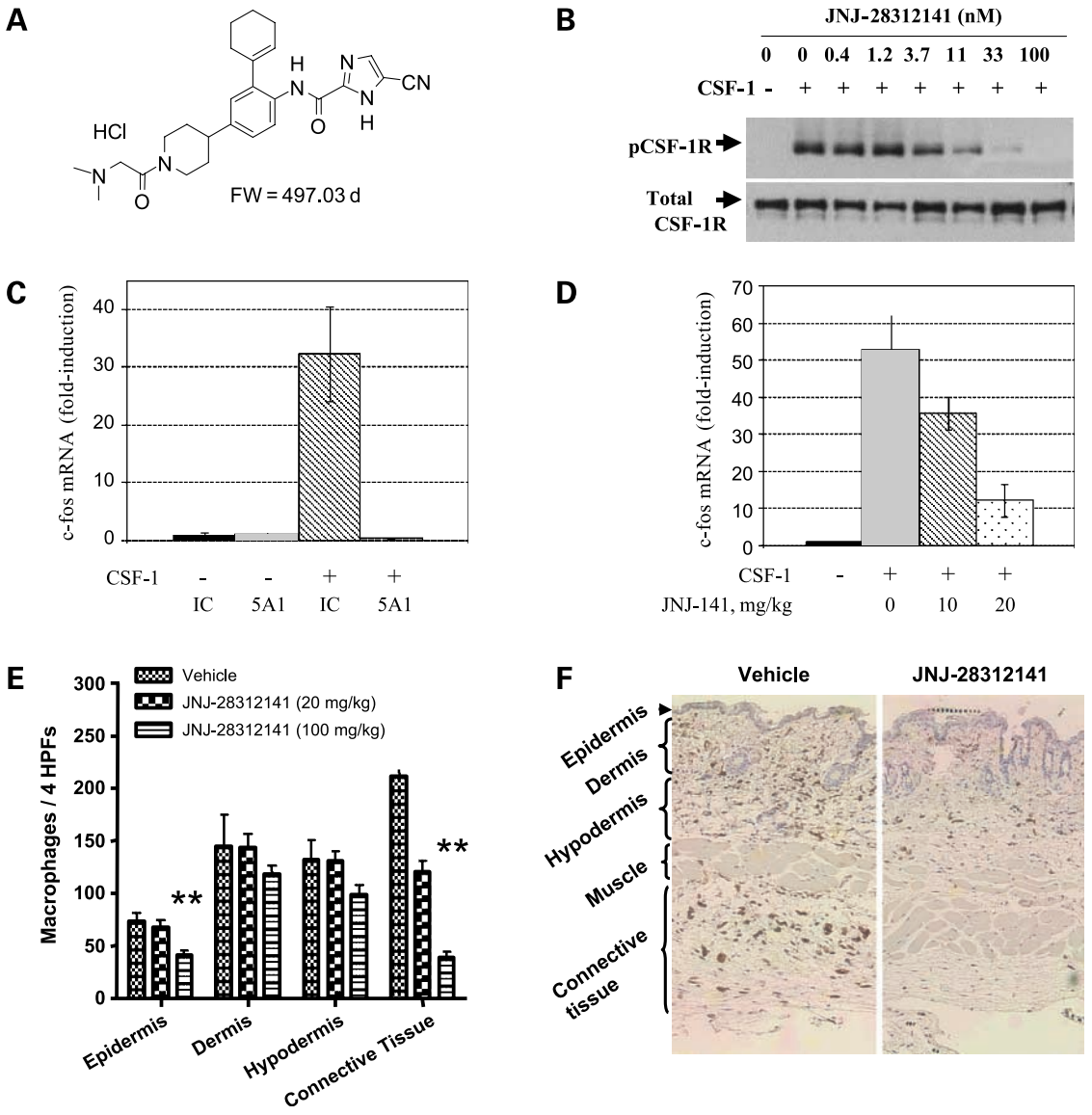

Figure 1. Structure and activity of JNJ-28312141. **A,** structure of JNJ-28312141. **B,** CSF-1R-HEK cells were pretreated 30 min with JNJ-28312141 and treated 10 min with 25 ng CSF-1/mL. Cell lysates were evaluated for phosphorylated CSF-1R and for total CSF-1R by immunoblot analysis. **C,** mice were dosed i.p. with 0.2 μg of rat monoclonal anti-mouse CSF-1 antibody (*5A1*) or with 0.2 μg of isotype control (*IC*) 8 h before tail-vein injection with saline alone or saline with 0.8 μg CSF-1. Fifteen minutes later, mice were sacrificed and c-fos mRNA was measured in spleen lysates as described in Materials and Methods. **D,** mice were dosed p.o. with vehicle (20% HPβCD) or with 10 or 20 mg/kg JNJ-28312141 8 h before tail-vein injection of saline alone or saline with 0.8 μg CSF-1. Fifteen minutes later, mice were sacrificed and c-fos mRNA was measured in spleen lysates as described in Materials and Methods. **E,** groups of five mice were dosed p.o. twice a day for 4 d with vehicle (20% HPβCD) or with 20 or 100 mg/kg JNJ-28312141. On day 5, mice were sacrificed and full thickness dorsal skin was processed for F4/80 immunohistochemistry as described for H460 tumors in Materials and Methods. F4/80 positive macrophages were counted in the epidermis, dermis, hypodermis, and s.c. layer. For each mouse, four representative fields (200×) of each layer were counted and summed. Summed counts were averaged to determine group mean and SEM values. JNJ-28312141 depleted macrophages in the epidermis and s.c. connective tissue (*$P < 0.05$ versus vehicle). **F,** representative F4/80-stained skin sections from a vehicle (*left*) and a JNJ-28312141 (100 mg/kg)–treated (*right*) mouse.

Published OnlineFirst November 3, 2009; DOI: 10.1158/1535-7163.MCT-09-0255

versus 115 other kinases was examined. Ninety-eight kinases were not inhibited 50% at 1 μmol/L (see Supplementary Table S1). Of the remaining kinases, five kinases had IC_{50} values of <0.1 μmol/L, including KIT (0.005 μmol/L), AXL (0.012 μmol/L), TRKA (0.015 μmol/L), FLT3 (0.030 μmol/L), and LCK (0.088 μmol/L).

In HEK cells transfected to express CSF-1R, JNJ-28312141 inhibited CSF-1–induced CSF-1R phosphorylation with an IC_{50} of 0.005 μmol/L (Fig. 1B). In primary cells, JNJ-28312141 inhibited CSF-1–dependent proliferation of mouse macrophages and CSF-1–induced expression of MCP-1 by human monocytes with IC_{50} values of 0.003 μmol/L. Seven-fold higher concentrations of JNJ-28312141 inhibited the ITD-FLT3–dependent proliferation of MV-4-11 cells (IC_{50}, 0.021 μmol/L), and higher concentrations inhibited FLT3 ligand–induced FLT3 phosphorylation in recombinant Baf3 cells (IC_{50}, 0.076 μmol/L), KIT-dependent proliferation of Mo7e cells (IC_{50}, 0.041 μmol/L), and TRKA-dependent proliferation of TF-1 cells (IC_{50}, 0.15 μmol/L). Despite the potent inhibition of LCK and AXL in recombinant kinase assays, only high (>2 μmol/L) concentrations inhibited these targets in cellular assays (see Supplementary Table S3). Furthermore, JNJ-28312141 (5 μmol/L) did not inhibit the growth factor–independent proliferation of H460, MDA-MB-231, or A375 adenocarcinoma cells. In total, the data identified JNJ-28312141 as a potent inhibitor of CSF-1R with additional functional activity at FLT3 and KIT in cells at nanomolar concentrations.

In vivo Pharmacodynamic Activity of JNJ-28312141

JNJ-28312141 was assessed *in vivo* using a simple pharmacodynamic model. After i.v. administration of recombinant CSF-1 to mice, c-fos mRNA in spleens was induced within 15 minutes but returned to baseline by 30 minutes. Induction was CSF-1 dose-dependent (ED_{50} ca. 0.8 μg/mouse; data not shown) and blocked completely in mice dosed with a CSF-1–neutralizing monoclonal antibody (Fig. 1C). When given 8 hours before CSF-1 challenge, a p.o. dose of 20 mg/kg JNJ-28312141 blocked c-fos mRNA induction significantly, albeit partly (Fig. 1D), showing the potential of doses ≥20 mg/kg to suppress CSF-1R signaling in mice.

CSF-1 is a survival factor for macrophages resident in several tissues including the skin (13–15). To identify doses of JNJ-28312141 capable of depleting CSF-1R–dependent macrophages, mice were dosed twice daily for 4 days, and macrophages in skin sections were counted (Fig. 1E and F). Macrophages in the s.c. connective tissue were depleted by 45% and 80% by 20 and 100 mg/kg JNJ-28312141, respectively. Macrophages present in the epidermis were reduced significantly by 100 mg/kg JNJ-28312141. In contrast to the low numbers of skin macrophages reported in CSF-1R-null mice, CSF-1R-null mice have moderate numbers of hepatic macrophages that are reduced roughly 50% when compared with wild-type mice (15). In a separate study (Supplementary Fig. S1), JNJ-28312141 reduced hepatic macrophage numbers in wild-type mice by 40% but had no effect on hepatic macrophage numbers in CSF-1R-null mice. These data were consistent with a role for CSF-1R inhibition in macrophage depletion by JNJ-28312141.

JNJ-28312141 Suppressed the Growth of H460 Non–Small Cell Lung Adenocarcinoma Xenografts

Next, we used JNJ-28312141 to test the hypothesis that CSF-1R–dependent macrophages may support the growth of some solid tumors. First, tumor xenograft models of diverse tissue origins (breast MDA-MB-231, breast SKOV3, lung H460, melanoma A375, and colon SW620) were assessed for potential CSF-1–macrophage circuits. Robust levels of human CSF-1 protein were detected by ELISA in lysates of each tumor xenograft (e.g., 35 ng CSF-1/g H460 tumor; see Supplementary Table S4). Furthermore, all tumor xenografts were characterized by moderate to high numbers of macrophages in the tumor stroma and smaller numbers of macrophages within fields dominated by tumor cells. To minimize the potential for direct JNJ-28312141 antitumor activity, H460 xenografts were selected for further studies because human CSF-1R mRNA was not detectable in H460 tumors by reverse transcription–PCR (data not shown).

In contrast to the inability of JNJ-28312141 to reduce growth of H460 cells in culture, p.o. administration of JNJ-28312141 reduced the growth rates of H460 tumors in a dose-dependent fashion (Fig. 2A). At study termination, average tumor weights were reduced by 21%, 32%, and 45% in mice dosed with 25, 50, and 100 mg/kg JNJ-28312141, respectively (Table 1). No overt toxicity or adverse effects on body weight were observed during the treatment period.

Tumor Growth Suppression Was Associated with Loss of TAMs and Vascularity and Elevated Plasma CSF-1

TAMS were abundant in the tumor stroma of vehicle-treated mice (Fig. 2B) and were present in lower numbers within regions dominated by tumor cells. JNJ-28312141 efficiently reduced TAM numbers in a dose-dependent fashion (Table 1) and depleted TAMs markedly at the 100 mg/kg dose (Fig. 2B). Because TAMs may contribute to tumor angiogenesis, $CD31^+$ microvasculature was also assessed (Fig. 2B; Table 1). JNJ-28312141 dose-dependently reduced tumor vascularity with a 66% reduction at the highest dose.

Hepatic sinusoidal macrophages clear CSF-1 from plasma by CSF-1R-mediated cellular internalization (33) that is dependent partly on CSF-1R kinase activity (34). Human (tumor-derived) CSF-1 was undetectable in plasma of vehicle-treated mice (Table 1) despite high expression of CSF-1 by the tumors. In contrast, human CSF-1 was detected in plasma of JNJ-28312141–treated mice and was increased sharply in a dose-dependent manner. JNJ-28312141 also caused murine CSF-1 to increase in plasma. These elevations may reflect CSF-1R kinase inhibition as suggested (35).

Inhibition of Osteoclastogenesis and Osteolysis by JNJ-28312141 in a Rat Model of Metastatic Bone Disease

Bone erosion is a source of morbidity in patients with metastatic bone disease despite treatment with bisphosphonates, such as zoledronate. Because CSF-1 is required for osteoclastogenesis, we compared JNJ-28312141 to zoledronate in a model of bone metastasis. After inoculation of syngeneic MRMT mammary carcinoma cells into the tibiae of rats, tumors filled the marrow cavity and activated a

Published OnlineFirst November 3, 2009; DOI: 10.1158/1535-7163.MCT-09-0255

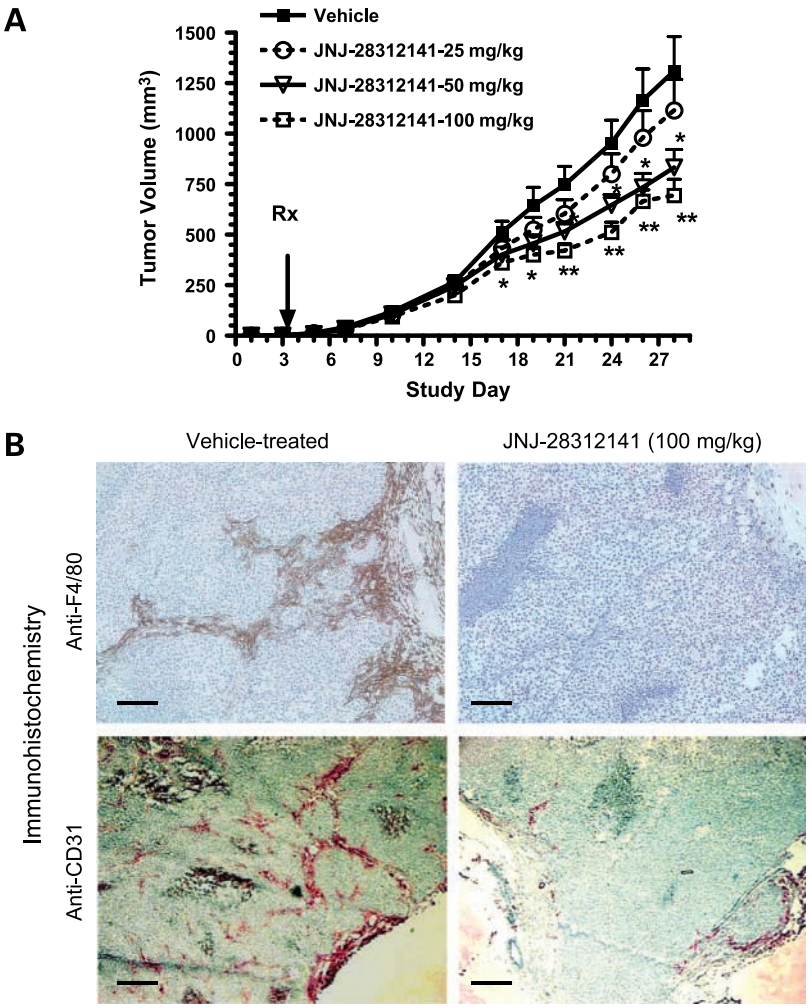

Figure 2. JNJ-28312141 reduced the growth, TAMs, and microvascularity of H460 xenografts. Three days after s.c. inoculation of nude mice with H460 cells, p.o. dosing was initiated with vehicle or 25, 50, or 100 mg/kg JNJ-28312141. Dosing was twice daily during the week and once daily on weekends for 25 consecutive days. **A,** tumor volumes were determined by caliper measurement. *Points,* means; *bars,* SEMs. *, $P < 0.05$ versus the vehicle control. **, $P < 0.01$ versus the vehicle control. **B,** day 28 tumors were harvested from vehicle-treated mice (*left column*) or mice treated with 100 mg/kg JNJ-28312141 (*right column*). Tumor sections were stained for F4/80$^+$ macrophages (*top row*, 40× magnification; *bar,* 100 μm) or for CD31$^+$ microvasculature (*bottom row*, 20× magnification; *bar,* 200 μm) as described in Materials and Methods.

program of osteolysis. By day 17, microradiography, microcomputed tomography, and histology indicated extensive loss of trabecular bone and full thickness cortical lesions in all vehicle-treated rats (Table 2; Fig. 3). In contrast, tibiae were well preserved in rats treated with 20 or 60 mg/kg JNJ-28312141. Radiographic erosions, if detectable at all, were limited to one to three small radiolucent lesions. JNJ-28312141 reduced trabecular erosions, and overall trabecular bone area in rats dosed with JNJ-28312141 was not different from sham (tumor-free) rats. The effect of

Table 1. JNJ-28312141 reduced the growth of H460 tumors, diminished TAMs and microvasculature, and elevated plasma CSF-1

Dose* JNJ-28312141, mg/kg	JNJ-28312141 plasma levels†, ng/mL	Mean final tumor weight, mg	Macrophage density, % area‡	Microvascular density, % area§	Plasma CSF-1, pg/mL (human)	Plasma CSF-1, pg/mL (mouse)
0	0	1,584 ± 257	10.6 ± 1.83	3.66 ± 0.85	0	1,345 ± 63
25	243 ± 37	1,257 ± 209	4.3 ± 0.68‖	3.73 ± 0.81	217 ± 89¶	1,770 ± 73¶
50	594 ± 44	1,070 ± 121	2.6 ± 0.57‖	2.10 ± 0.57	396 ± 76‖	1,722 ± 98
100	1159 ± 77	870 ± 94¶	0.31 ± 0.14‖	1.25 ± 0.16¶	778 ± 253‖	2,293 ± 88‖

NOTE: Values represent means ± SEM ($n = 15$).
*Twice daily (except once daily on weekends) oral dosing commenced 3 d after s.c. inoculation of H460 lung adenocarcinom cells and continued until sacrifice on day 28.
†Plasma levels of JNJ-28312141 were determined 2 h after the final dose administration on day 28.
‡Percentage of area determined to be F4/80 positive.
§Percentage of area determined to be CD31 positive.
‖$P < 0.01$ versus control.
¶$P < 0.05$ versus control.

Published OnlineFirst November 3, 2009; DOI: 10.1158/1535-7163.MCT-09-0255

Table 2. JNJ-28312141 inhibited MRMT-1 tumor–induced bone erosions and osteoclastogenesis

Treatment*	JNJ-28312141 plasma levels†, ng/mL	Microradiograph score‡	Trabecular bone volume score§	Osteoclast counts‖	Tumor volume score§
No cells	0	0	2.29 ± 0.31	-	-
MRMT + vehicle	0	3.88 ± 0.24	0.88 ± 0.13	58.0 ± 5.6	3.00 ± 0
MRMT + JNJ-28312141, 20 mpk	822 ± 9	0.75 ± 0.17¶	2.00 ± 0.0.2¶	3.7 ± 0.7¶	1.75 ± 0.48**
MRMT + JNJ-28312141, 60 mpk	2470 ± 443	0.83 ± 0.18¶	2.33 ± 0.23¶	2.6 ± 1.5¶	1.50 ± 0.55**
MRMT + zoledronate, 0.03 mpk	0	0.38 ± 0.20¶	2.63 ± 0.20¶	21.0 ± 3.2¶	1.63 ± 0.20¶

NOTE: Values represent means ± SEM (n = 8).

*On day 0, saline (no cells) or saline containing 3×10^4 MRMT-1 rat mammary gland carcinoma cells was injected into the medullary cavity of the right proximal tibia. Twice-daily oral dosing with vehicle or with 20 or 60 mg/kg JNJ-28312141 or once every other day s.c. dosing with 0.03 mg/kg zoledronate commenced on day 3 until sacrifice on day 17.

†Plasma levels of JNJ-28312141 were determined 2 h after the final dose administration.

‡Values based on five-point visual score described in Materials and Methods.

§Values based on three-point visual score described in Materials and Methods.

‖Mean number of TRAP$^+$ cells in three 200× fields where numbers of tumor-associated osteoclasts were greatest.

¶$P < 0.01$ versus control.

**$P < 0.05$ versus control.

JNJ-28312141 on radiographic scores was similar to zoledronate. However, zoledronate blocked normal remodeling of trabecular bone at the growth plate and caused a trend toward increased trabecular bone area. Regardless of treatment, marrow cavities of nearly all tumor-inoculated rats were filled with necrotic tumor but viable tumor tissue (presumed to arise from draining lymph nodes) began to encapsulate the tibia. JNJ-28312141 or zoledronate reduced the size of the encapsulating tumors measured on day 17. In vehicle-treated rats, large, multinucleated TRAP$^+$ osteoclasts were abundant in the tumors and lined residual bone surfaces (Fig. 3; Table 2). Tumor-associated osteoclasts were reduced by 64% by zoledronate. In contrast, TRAP$^+$ tumor-associated osteoclasts were reduced ca. 95% by JNJ-28312141. Concentrations of JNJ-28312141 in plasma that were associated with marked osteoclast reductions in the MRMT-1 model at 20 mg/kg were comparable with concentrations associated with macrophage reductions in H460 xenografts in mice dosed with 50 to 100 mg/kg (Tables 1 and 2). Higher doses were required in mice due to a shorter compound half-life in this species (i.e., compound half-life was 3.4 hours in mice and 5.8 hours in rats).

JNJ-28312141 Caused Regression of ITD-FLT3–Dependent MV-4-11 AML Xenografts

Constitutively active FLT3 mutants are found in approximately one third of AML patients (25, 27), and some of these have responded to experimental FLT3 kinase inhibitors (27). Because JNJ-28312141 inhibited the proliferation of ITD-FLT3–dependent MV-4-11 AML cells with nanomolar potency, we examined JNJ-28312141 for ability to regress MV-4-11 xenografts. Established MV-4-11 tumors regressed completely in mice dosed twice daily with 50 or 100 mg/kg JNJ-28312141 (Fig. 4A).

To determine if JNJ-28312141 inhibited FLT3 kinase in MV-4-11 tumors, mice in the vehicle-treated group bearing large tumors were randomized on day 12 and dosed a single time with vehicle or with a single inefficacious (10 mg/kg) or efficacious (100 mg/kg) dose of JNJ-28312141 (Fig. 4B). Six hours later, tumor FLT3 phosphorylation was substantially reduced in mice receiving a dose of 100 mg/kg JNJ-28312141, but FLT3 phosphorylation was only reduced mildly in mice dosed with 10 mg/kg JNJ-28312141 (Fig. 4B).

To assess the durability of the JNJ-28312141–induced antitumor effect, mice (n = 15) in the 100 mg/kg dose group were taken off JNJ-28312141 treatment on study day 12 and kept alive to allow the tumors in these mice to regrow (Fig. 4C). In general, tumor regrowth was slow and varied considerably within this group of mice. Individual mice were terminated on days 32 (two mice), 39, 41, and 46 when tumors exceeded 1,000 mm^3. All mice were terminated on day 46, at which time seven mice still had no palpable tumor mass and four mice had measurable tumors <500 mm^3.

Discussion

Herein, we have described JNJ-28312141, a novel small-molecule inhibitor of CSF-1R kinase with a narrow selectivity profile and with preclinical activities in a variety of cancer settings. These data, together with a recent report by Kubota et al. (9), illustrate the potential for selective small molecule inhibitors of CSF-1R to reduce TAMs, tumor angiogenesis, and solid tumor growth.

JNJ-28312141 inhibited CSF-1–induced proliferation of murine macrophages, and p.o. doses of JNJ-28312141 blocked CSF-1–induced c-fos expression and caused the loss of CSF-1–dependent skin macrophages. We therefore used JNJ-28312141 to examine the hypothesis that CSF-1R–dependent macrophages may support the growth of some solid tumors. In an H460 tumor xenograft model, JNJ-28312141 produced dose-dependent growth suppression accompanied by dose-dependent decreases in TAMs and tumor microvasculature. These events occurred over a dose range that produced increasing loses of CSF-1–dependent

Published OnlineFirst November 3, 2009; DOI: 10.1158/1535-7163.MCT-09-0255

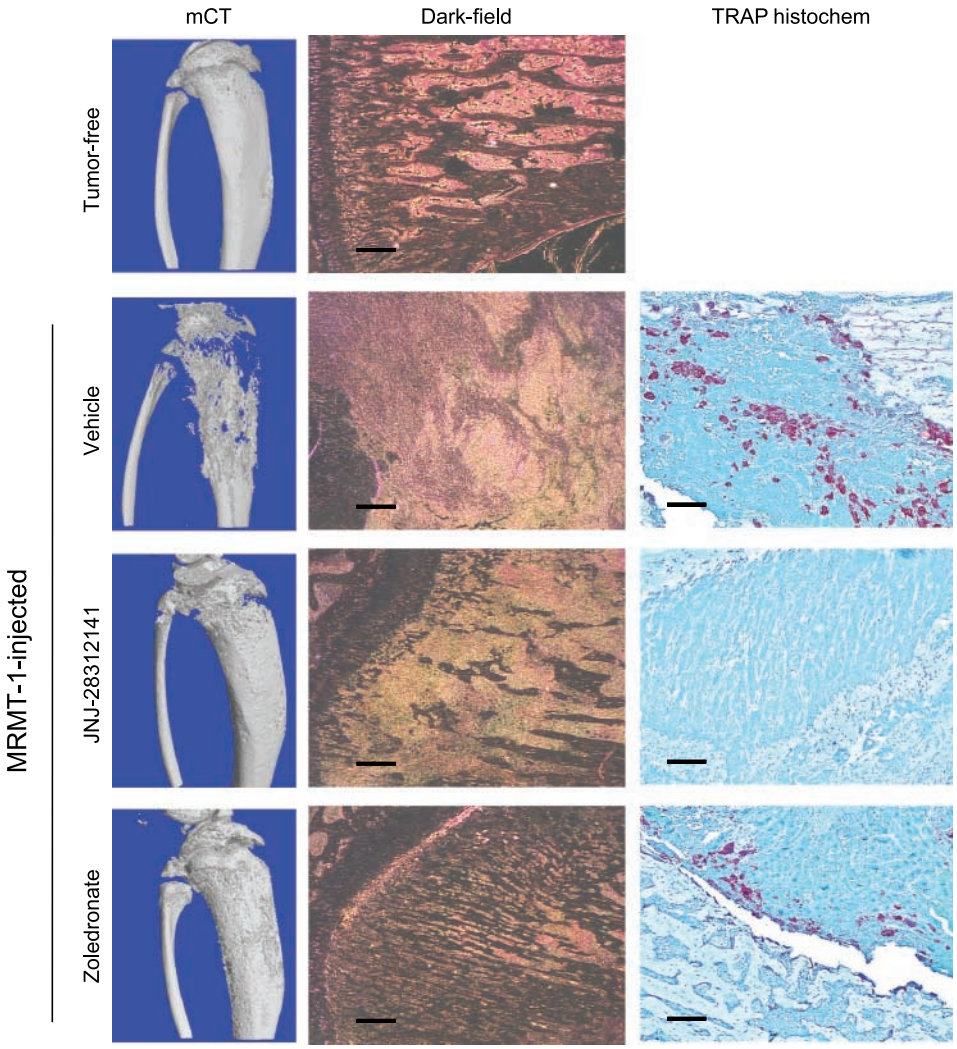

Figure 3. JNJ-28312141 prevented MRMT-1 tumor-induced osteoclastogenesis and bone erosion. Saline (*top row*) or MRMT-1 cells (*bottom three rows*) were inoculated into the right tibia of SD rats. Starting 3 d later until sacrifice on day 17, rats were dosed p.o. twice daily with vehicle (*second row*) or with 20 mg/kg JNJ-28312141 (*third row*) or every other day with 0.030 mg/kg zoledronate s.c. (*bottom row*). On day 17, rats were sacrificed and right hind limbs were scored by microradiography (Table 2). Representative tibiae were imaged further by microcomputed tomography (*left column*). *Center column,* representative histologic sections were photographed at 40× magnification under dark field illumination to visualize trabecular bone below the growth plate (epiphyseal growth plate is oriented along the left margin of each photomicrograph). *Bar,* 100 μm. *Right column,* sections were stained for $TRAP^+$ cells. Representative areas of tumor adjacent to bone were photographed at 40× magnification. *Bar,* 100 μm.

macrophages in normal skin and graded increases in plasma CSF-1. Plasma CSF-1 is cleared by a CSF-1R–dependent mechanism (33) and is elevated in CSF-1R-null mice (15). Ki20227, a CSF-1R inhibitor that is structurally unrelated to JNJ-28312141, was also associated with elevated plasma CSF-1 (35), and plasma CSF-1 elevations may be considered a possible functional marker of CSF-1R kinase inhibition. The increases in plasma CSF-1 and the decreases in TAMs over the dose range used in the current study are consistent with a causal relationship between CSF-1R inhibition and tumor growth inhibition, although we cannot exclude contributions from other targeted activities. A direct effect of JNJ-8312141 on H460 cells was unlikely because H460 tumors did not express human CSF-1R, and proliferation of H460 cells in culture was not inhibited by JNJ-28312141.

Reduced H460 tumor growth was associated with reduced tumor vessel density. The ability of oral JNJ-28312141 to suppress tumor growth and vessel density was consistent with a growing body of literature that macrophages are required for optimal tumor angiogenesis. For example, depletion of TAMs by parenteral injection of liposomal clodronate suppressed tumor xenograft growth and prevented tumor angiogenesis more effectively than anti–vascular endothelial growth factor (8). In a transgenic mouse susceptible to mammary cancer, macrophage recruitment preceded the formation of high-density vessel networks, but macrophage recruitment and tumor vessel network formation were greatly delayed and reduced in CSF-1–deficient mice (6). Others have reported that parenterally given CSF-1 antibody and CSF-1 antisense oligonucleotides reduced tumor-associated endothelial cell proliferation together with an ~50% growth suppression of mammary and colon carcinoma xenografts accompanied by substantial extensions in survival (10–12). Although tumors continued to grow in the presence of CSF-1/CSF-1R inhibition, this was also true of similar xenografts after treatment with bevacizumab, a vascular endothelial growth factor antibody in current clinical use to treat breast and colon cancer in combination with standard therapy (36). Of note, survival benefits provided by CSF-1 antibody was more

Published OnlineFirst November 3, 2009; DOI: 10.1158/1535-7163.MCT-09-0255

than additive when combined with cytotoxic therapy, and we are currently testing JNJ-28312141 in combination studies to model the most likely clinical use of CSF-1R inhibitors.

More recently, treatment of mice with Ki20227, an alternative small molecule inhibitor of CSF-1R, reduced the formation of vessel networks in a transplantable model of osteosarcoma (9). An increase in plasma CSF-1 observed herein with JNJ-28312141 was observed previously with Ki20227 (35) and raises concerns about potential rebound effects upon dose cessation. Although further study of this issue is needed, osteosarcomas in mice treated with Ki20227 exhibited a disorganized vasculature matrix, and cessation of Ki20227 administration did not result in rapid vascular regrowth or in a reduction in survival benefit (9).

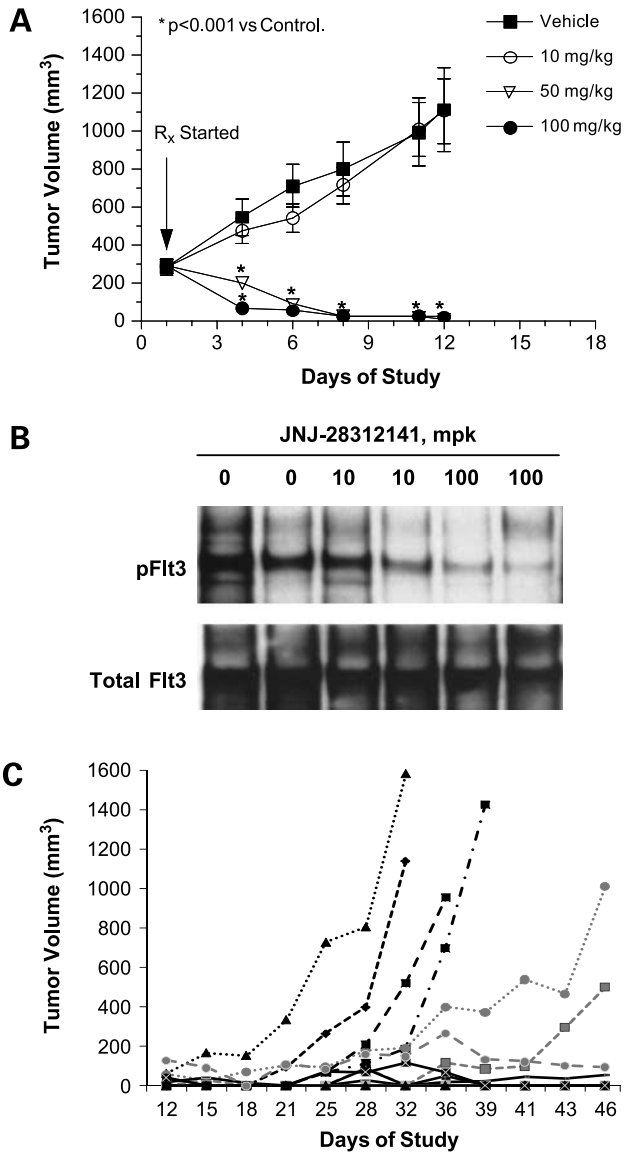

Figure 4. JNJ-28312141 induced regression of MV-4-11 xenografts. **A,** MV-4-11 cells were inoculated s.c. into nude mice. When mean tumor volume reached 288 mm^3, twice daily p.o. dosing was initiated with vehicle or 10, 50, or 100 mg/kg JNJ-28312141 for 11 d, and tumor volumes were measured with a caliper. **B,** on day 12, vehicle-treated mice were given a single additional dose of vehicle or a single 10 or 100 mg/kg dose of JNJ-28312141. Six hours later mice were sacrificed, tumors were isolated and homogenized, and pFLT3 and FLT3 were assessed in tumor lysates by immunoprecipitation and Western blotting as described in Materials and Methods. **C,** mice in the 100 mg/kg dose group were taken off treatment on study day 12 and kept alive to assess tumor regrowth. Tumor volumes were measured twice or thrice a week until day 46, and the growth of tumors in individual mice is shown. Tumor regrowth was detected in 8 of 15 mice. Data on seven mice are not visible in the graph because tumor volumes were at baseline (undetectable).

H460 cells were derived from a non–small cell lung cancer, and clinical evidence suggests the potential for CSF-1–macrophage circuits in this cancer type. For example, serum CSF-1 was reported to increase during non–small cell lung cancer progression and was a predictor of poor survival (21), as were TAM numbers (37). However, CSF-1 is elevated in clinical biopsies (18) and serum in patients with a variety of malignancies (19–21, 38). Furthermore, anti–CSF-1 antisense and antibody strategies were efficacious in preclinical models of breast, colon, and germinal neoplasias (10–12), and Ki20227 was efficacious in an osteosarcoma model (9). Collectively, these data suggest a general role for CSF-1 in TAM recruitment and solid tumor growth in multiple tumor types, and CSF-1R inhibitors may have broad therapeutic applicability.

As observed with previous compounds that inhibit FLT3 (26), JNJ-28312141 induced complete regression of ITD-FLT3–dependent MV-4-11 AML xenografts in nude mice. Among the several FLT3 compounds described to date, JNJ-28312141 is distinguished by CSF-1R potency. Many AML leukemias are positive for CSF-1R, express autocrine CSF-1, and exhibit constitutive CSF-1R phosphorylation (39). CSF-1 levels are elevated in AML patients (38), and CSF-1R expression is a negative prognostic factor (40). Because CSF-1R has oncogenic potential (41), the role of CSF-1R in AML and in other cancers merits further study. New therapeutics in AML must avoid hematologic toxicity, and mouse genetics suggest dual inhibition of FLT3 and KIT may suppress blood cell production (42). However, JNJ-28312141 has been well tolerated in subacute studies in rats, and hematologic toxicity of Sutent has been manageable in cancer patients despite demonstrable inhibition of FLT3 and KIT at therapeutic doses (43).

JNJ-28312141 reduced tumor growth and markedly reduced bone erosion and tumor-associated osteoclasts in a MRMT-1 model of metastatic bone disease. Currently the bisphosphonate zoledronate is indicated for the prevention of skeletal events in patients with bone metastasis (44), and denosumab, a RANK ligand antibody, has shown good ability to reduce skeletal events in clinical trials (45). Nonetheless, many patients experience skeletal events despite these therapies, and some patients may benefit from agents with an alternative mechanism of action or from combination therapy. Bisphosphonates are rapidly acting osteoclast toxins. In contrast CSF-1R inhibitors block the formation of new osteoclasts (46). Although zoledronate afforded excellent bone protection in the MRMT-1 model, many tumor-associated osteoclasts remained evident in zoledronate-treated rats. In contrast, tumor-associated osteoclasts were rare in

Published OnlineFirst November 3, 2009; DOI: 10.1158/1535-7163.MCT-09-0255

JNJ-28312141-treated rats, suggesting CSF-1R inhibitors, such as JNJ-28312141, may have powerful bone sparing effects, particularly when dosed chronically. These data provide the first comparison of a CSF-1R inhibitor with zoledronate in a model with direct tumor inoculation into bone and confirm and extend previous reports of bone protection by an alternative selective CSF-1R kinase inhibitor, Ki20227, after intracardiac tumor inoculation (46). CSF-1R inhibitors provide a novel mechanism to suppress growth of secondary tumors residing not only in bone but also in soft tissue and together, the data support therapeutic testing of CSF-1R inhibitors in the treatment of the many patients diagnosed with bone metastases that are at risk of fracture, bone pain, and hypercalcemia.

Multitargeted kinase inhibitors including sunitinib and imatinib have been reported in the literature to include CSF-1R in their target profile (47). However, these later compounds are dose limited by tolerability, and it is not known to what extent CSF-1R is inhibited at prescribed doses. JNJ-28312141 is representative of several more recently described potent small molecule inhibitors of CSF-1R with improved selectivity (47). We anticipate that compounds with focused CSF-1R selectivity will have improved tolerability permitting greater flexibility in chronic dosing regimens as patient life expectancy increases. In addition to reducing tumor growth and tumor-associated bone lesions, further studies are needed to assess the potential of CSF-1R inhibitors to enhance chemo- and radiotherapy and to enhance the activity of other antiangiogenesis agents. Furthermore, because mouse genetics identified a role for CSF-1 in metastasis (6) and because CSF-1R antibody caused marked reductions in tumor cell intravasation (48), CSF-1R inhibitors may ultimately prove useful in preventing tumor cell egress and the metastatic dissemination that contributes to the demise of cancer patients.

Disclosure of Potential Conflicts of Interest

Authors are employees of Johnson & Johnson Pharmaceutical Research & Development, L.L.C.

Acknowledgments

We thank David End for critical review of this manuscript and Dan Small and Steve Bain (MDS Pharma Services) for performing the MRMT-1 bone metastasis model.

References

1. Wood GW, Gollahon KA. Detection and quantitation of macrophage infiltration into primary human tumors with the use of cell-surface markers. J Natl Cancer Inst 1977;59:1081–7.

2. Bingle L, Brown NJ, Lewis CE. The role of tumour-associated macrophages in tumour progression: implications for new anticancer therapies. J Pathol 2002;196:254–65.

3. Sica A, Larghi P, Mancino A, et al. Macrophage polarization in tumor progression. Semin Cancer Biol 2008;18:349–55.

4. Biswas SK, Sica A, Lewis CE. Plasticity of macrophage function during tumor progression: regulation by distinct molecular mechanisms. J Immunol 2008;180:2011–7.

5. Pollard JW. Macrophages define the invasive microenvironment in breast cancer. J Leukoc Biol 2008;84:623–30.

6. Lin EY, Li J-F, Gnatovskiy L, et al. Macrophages regulate the angiogenic switch in a mouse model of breast cancer. Cancer Res 2006;66:11238–46.

7. Nowicki A, Szenajch J, Ostrowska G. Impaired tumor growth in colony-stimulating factor 1 (CSF-1)-deficient, macrophage-deficient op/op mouse: evidence for a role of CSF-1-dependent macrophages in formation of tumor stroma. Int J Cancer 1996;65:112–9.

8. Zeisberger SM, Odermatt B, Marty C, Zehnder-Fjallman AHM, Ballmer-Hofer K, Schwendener RA. Clodronate-liposome-mediated depletion of tumour-associated macrophages: a new and highly effective antiangiogenic therapy approach. Brit J Cancer 2006;95:272–81.

9. Kubota Y, Takubo K, Shimuzu T, et al. M-CSF inhibition selectively targets pathological angiogenesis and lymphangiogenesis. J Exp Med 2009;206:1089–102.

10. Aharinejad S, Abraham D, Paulus P, et al. Colony-stimulating factor-1 antisense treatment suppresses growth of human tumor xenografts in mice. Cancer Res 2002;62:5317–24.

11. Aharinejad S, Paulus P, Sioud M, et al. Colony-stimulating factor-1 blockade by antisense oligonucleotides and small interfering RNAs suppresses growth of human mammary tumor xenografts in mice. Cancer Res 2004;64:5378–5384.

12. Paulus P, Stanley ER, Schafer R, Abraham D, Aharinejad S. Colony-stimulating factor-1 antibody reverses chemoresistance in human MCF-7 breast cancer xenografts. Cancer Res 2006;66:4349–56.

13. Chitu V, Stanley ER. Colony-stimulating factor-1 in immunity and inflammation. Curr Opin Immunol 2006;18:39–48.

14. Pollard JW, Stanley ER. Pleotropic roles for CSF-1 in development defined by the mouse mutation osteopetrotic (op). Adv in Devel Biochem 1995;4:153–93.

15. Dai XM, Ryan GR, Hapel AJ, et al. Targeted disruption of the mouse colony-stimulating factor 1 receptor gene results in osteopetrosis, mononuclear phagocyte deficiency, increased primitive progenitor cell frequencies, and reproductive defects. Blood 2002;99:111–20.

16. Okazaki T, Ebihara S, Takahashi H, Asada M, Kanda A, Sasaki H. Macrophage colony-stimulating factor induces vascular endothelial growth factor production in skeletal muscle and promotes tumor angiogenesis. J Immunol 2005;174:7531–8.

17. Rosen LS, Gordon D, Kaminski M, et al. Long-term efficacy and safety of zoledronic acid compared with pamidronate disodium in the treatment of skeletal complications in patients with advanced multiple myeloma or breast carcinoma. Cancer 2003;98:1735–44.

18. Kascinski B. Expression of CSF-1 and its receptor CSF-1R in non-hematopoietic neoplasms. Cancer Treat Res 2002;107:285–92.

19. Ide H, Hatake K, Terado Y, et al. Serum level of macrophage colony-stimulating factor is increased in prostate cancer patients with bone metastasis. Human Cell 2008;21:1–6.

20. McDernitt RS, Deneux L, Mosseri V, et al. Circulating macrophage colony stimulating factor as a marker of tumour progression. Eur Cytokine Netw 2002;13:121–7.

21. Kaminska J, Kowalsk M, Kotowicz B, et al. Pretreatment serum levels of cytokines and cytokine receptors in patients with non-small cell lung cancer, and correlations with clinicopathological features and prognosis. M-CSF — an independent prognostic factor. Oncology 2006;70:115–25.

22. Inhibitors of c-FMS Kinase. US Patent Application 2006: US 2006189623 A1.

23. Illig CR, Chen J, Wall MJ, et al. Discovery of novel FMS kinase inhibitors as anti-inflammatory agents. Bioorg Med Chem Lett 2008;18:1642–8.

24. Huang H, Hutta DA, Rinker JM, et al. Pyrido[2,3-*d*]pyrimidin-5-ones: a novel class of anti-inflammatory FMS inhibitors. J Med Chem 2009;52:1081–99.

25. Quentmeier H, Reinhardt J, Zaborski M, Drexler HG. Flt3 mutations in acute myeloid leukemia cell lines. Leukemia 2003;17:120–4.

26. O'Farrell AM, Abrams TJ, Yuen HA, et al. SU11248 is a novel FLT3 tyrosine kinase inhibitor with potent activity *in vitro* and *in vivo*. Blood 2003;101:3597–605.

27. Small D. Targeting FLT3 for the treatment of leukemia. Semin Hematol 2008;45:S17–21.

28. Schalk-Hihi C, Ma H-C, Struble GT, et al. Protein engineering of the colony stimulating factor 1 receptor kinase domain for structural studies. J Biol Chem 2007;208:4085–93.

29. Baumann CA, Zeng L, Donatelli RR, Maroney AC. Development of a

Published OnlineFirst November 3, 2009; DOI: 10.1158/1535-7163.MCT-09-0255

quantitative, high-throughput cell-based enzyme-linked immunosorbent assay for detection of colony-stimulating factor-1 receptor tyrosine kinase inhibitors. J Biochem Biophys Methods 2004;60:69–79.

30. Roudier MP, Bain SD, Dougall WC. Effects of the RANKL inhibitor, osteoprotegerin, on the pain and histopathology of bone cancer in rats. Clin Exp Metastasis 2006;23:167–75.

31. Walker K, Medhurst SJ, Kidd BL, et al. Disease modifying and anti-nociceptive effects of the bisphosphonate, zoledronic acid in a model of bone cancer pain. Pain 2002;100:219–29.

32. Liu C, Sanghvi R, Burnell JM, Howard GA. Simultaneous demonstration of bone alkaline and acid phosphatase activities in plastic-embedded sections and differential inhibition of the activities. Histochemistry 1987;86:559–65.

33. Bartocci A, Mastrogiannis DS, Migliorati G, Stockert RJ, Wolkoff WW, Stanley ER. Macrophages specifically regulate the concentration of their own growth factor in the circulation. Proc Natl Acad Sci U S A 1987;87:6179–83.

34. Carlberg K, Tapley P, Haystead C, Rohrschneider L. The role of kinase activity and the kinase insert region in ligand-induced internalization and degradation of the c-fms protein. EMBO J 1991;10:877–83.

35. Ohno H, Uemura Y, Murooka H, et al. The orally-active and selective c-Fms tyrosine kinase inhibitor Ki20227 inhibits disease progression in a collagen-induced arthritis mouse model. Eur J Immunol 2008;38:283–91.

36. Kolinsky K, Shen B-Q, Zhang Y-E, et al. *In vivo* activity of novel capecitabine regimens alone and with bevacizumab and oxaliplatin in colorectal cancer xenograft models. Mol Cancer Ther 2009;8:75–82.

37. Chen JJW, Lin Y-C, Yao P-L, et al. Tumor-associated macrophages: the double-edged sword in cancer progression. J Clin Onc 2005;23:953–964.

38. Janowska-Wieczorek A, Belch AR, Jacobs A, et al. Increased circulating colony-stimulating factor-1 in patients with preleukemia, leukemia, and lymphoid malignancies. Blood 1991;77:1796–803.

39. Zheng R, Klang K, Gorin NC, Small D. Lack of kit or FMS internal tandem duplications but coexpression with ligands in AML. Leukemia Res 2004;28:121–6.

40. Muller-Tidow C, Schwable J, Steffen B, et al. High-throughput analysis of genome-wide receptor tyrosine kinase expression in human cancers identifies potential novel drug targets. Clin Cancer Res 2004;10:1241–9.

41. Kirma N, Luthra R, Jones J, et al. Overexpression of the colony-stimulating factor (CSF-1) and/or its receptor c-fms in mammary glands of transgenic mice results in hyperplasia and tumor formation. Cancer Res 2004;64:4162–70.

42. Mackarehtschian K, Hardin JD, Moore KA, Boast S, Goff SP, Lemischka IR. Targeted disruption of the flk3/flt3 gene leads to deficiencies in primitive hematopoietic progenitors. Immunity 1995;3:147–61.

43. Faivre S, Delbaldo C, Vera K, et al. Safety, pharmacokinetic, and anti-tumor activity of SU11248, a novel oral multitarget tyrosine kinase inhibitor, in patients with cancer. J Clin Oncol 2006;24:25–35.

44. Body J-J. Breast cancer: bisphosphonate therapy for metastatic bone disease. Clin Cancer Res 2006;12:6258–63s.

45. Lipton A, Steger GG, Figueroa J, et al. Extended efficacy and safety of Denosumab in breast cancer patients with bone metastases not receiving prior bisphosphonate therapy. Clin Cancer Res 2008;14:6690–6.

46. Ohno H, Kubo K, Murooka H, et al. A c-fms tyrosine kinase inhibitor, Ki20227, suppresses osteoclast differentiation and osteolytic bone destruction in a bone metastasis model. Mol Cancer Ther 2006;5:2634–43.

47. Manthey CL, Player MR. Advances in the discovery of anti-inflammatory FMS Inhibitors. Annu Rep Med Chem 2009;44:211–25.

48. Wyckoff JB, Wang Y, Lin EY, et al. Direct visualization of macrophage-assisted tumor cell intravasation in mammary tumors. Cancer Res 2007;67:2649–56.